Polymer 156 (2018) 128–135

Contents lists available at ScienceDirect

Polymer

journal homepage: www.elsevier.com/locate/polymer

Tuning polyaniline nanostructures via end group substitutions and their morphology dependent electrochemical performances

Yong Ma[a,b,*], Mingliang Ma[c], Xunqian Yin[a], Qian Shao[d], Na Lu[e], Yining Feng[e], Yang Lu[f], Evan K. Wujcik[f], Xianmin Mai[g,**], Chao Wang[h,***], Zhanhu Guo[b,****]

[a] School of Material Science and Engineering, Shandong University of Science and Technology, Qingdao, 266590, PR China
[b] Integrated Composites Laboratory (ICL), Department of Chemical and Biomolecular Engineering, University of Tennessee, Knoxville, TN, 37996, USA
[c] School of Civil Engineering, Qingdao University of Technology, Qingdao, 266033, PR China
[d] School of Chemical and Environmental Engineering, Shandong University of Science and Technology, Qingdao, 266590, China
[e] Lyles School of Civil Engineering, School of Materials Engineering, Birck Nanotechnology Center, Purdue University, West Lafayette, IN, 47906, USA
[f] Materials Engineering and Nanosensor [MEAN] Laboratory, Department of Chemical and Biological Engineering, The University of Alabama, Tuscaloosa, USA
[g] School of Urban Planning and Architecture, Southwest Minzu University, Chengdu, 610041, China
[h] School of Materials Science and Engineering, North University of China, Taiyuan, 030051, China

HIGHLIGHTS

- The dimension of PANI was effectively tuned by varying the end groups of additive surfactants.
- PANI fiberboards, dendrites, and rods exhibited morphology dependent electrochemical properties.
- PANI rods exhibited higher specific capacitance (192 F g^{-1}) than fiberboards (55 F g^{-1}) and dendrites (64 F g^{-1}) at 3.0 A g^{-1}.

ARTICLE INFO

Keywords:
Polyaniline
Surfactants
Electrochemical performances

ABSTRACT

The dimension of polyaniline (PANI) is effectively tuned by changing the end groups of additive surfactants. PANI fiberboards, dendrites, and rods are separately obtained through the guidance of micelle soft templates formed by the corresponding surfactants, i.e., sodium dodecyl sulfonate (SDS), sodium lauryl sulfonate (SLS), and sodium dodecyl benzene sulfonate (SDBS). Detailed mechanistic studies reveal that PANI structures are fabricated from a bottom-up self-assembly process where one-dimensional (1D) nanostructures are aggregated into higher order architectures. Electrochemical properties of these PANI nanostructures are examined in details, and exhibit morphological dependence. The PANI rods having high specific surface area and rough surface favor more ions enter into their body contact with active sites. As a consequence, they have higher specific capacitance (192 F g^{-1}) than fiberboards (55 F g^{-1}) and dendrites (64 F g^{-1}) at 3.0 A g^{-1}. Varying the substituent of additive molecules is in a position to alter the dimension of PANI that plays a decisive role in resulting electrochemical performances. This strategy may control the dimension and the properties of other conducting polymers for future applications.

1. Introduction

With the increasing crisis of fossil energy consumption accompanied by environmental pollution, electrical energy storage devices are becoming more and more significant [1]. Supercapacitors have been considered as one of the innovations in this field, and they are receiving much attention due to fast delivery rate, high power density, and long cycle life [2–5]. Electrode materials, at the heart of supercapacitors, directly decide the practical properties [6–9]. Carbon-based materials including graphene, carbon nanotubes, porous carbon, etc., with

* Corresponding author. School of Material Science and Engineering, Shandong University of Science and Technology, Qingdao, 266590, PR China.
** Corresponding author.
*** Corresponding author.
**** Corresponding author.
E-mail addresses: courage2010@126.com, mayongfn@gmail.com (Y. Ma), maixianmin@foxmail.com (X. Mai), wangchao_nuc@126.com (C. Wang), zguo10@utk.edu (Z. Guo).

https://doi.org/10.1016/j.polymer.2018.09.051
Received 8 July 2018; Received in revised form 8 September 2018; Accepted 25 September 2018
Available online 03 October 2018
0032-3861/

specific surface areas as high as possible are applied to electrical double layer capacitors [10,11]. Towards pseudocapaitors, transition metal oxides and conducting polymers are employed [12,13], especially the latter increasingly plays an indispensable role.

The term conducting polymers conjure up images of materials that combine the ease of processability of polymers with the electrical properties of metal [14–16]. Among this family, polyaniline (PANI) has attracted widespread interest and been depolyed for wide applications, owing to its easy synthesis, environmental stability, adjustable electrical conductivity, and reversible acid/base doping/dedoping chemistry [17–20]. Recent progress in regulating and directing PANI morphology is quite remarkable. With the help of some intriguing methods like templates [21], interfacial polymerzation [22], and oligomer-assisted polymerization [23], PANI nanofibers were readily obtained. Besides, a lot of mutli-dimensional PANI structures were produced via the use of inductive agents (proteins, surfactants, organic dopants) or oxidative templates, such as nanospheres [24], flower-like superstructures [25], brain-like structures [26], helical nanofibers [27], nanorings and flat hollow capsules [28], and chain-like hollow spheres [29].

It is noticeable that the dimension and morphology of PANI can prominently affect the performances of the supercapacitors [30]. Due to the well-defined tubular nanostructures, PANI nanotubes doped with malic acid and citric acid possessed a specific capacitance of 658 and 617 F/g in 1.0 M H_2SO_4 solution at a current density of 0.10 A/g [31]. In addition, PANI often works as an auxiliary material in the supercapacitor electrode materials. Aligned PANI nanowires decorating onto tubular MoS_2 not only showed a specific capacitance of 552 F/g at 0.50 A/g, but also gave a rate capability of 82% from 0.50 to 30 A/g [32]. The core/shell $NiCo_2O_4$/PANI nanorod arrays exhibited a specific capacitance of 901 F/g at 1.0 A/g and a capacitance retention of 91% after 3000 cycles at 10 A/g [33]. In a separate study, three-dimensional (3D) ordered PANI/graphene bulk displayed a specific capacitance as high as 1225 F/g at 1.0 A/g, together with an outstanding cycling stability (85.7% of initial capacitance after 1500 cycles) [34]. However, the effects of PANI morphology on the final electrochemical properties have been rarely reported. Therefore, developing a reliable way of evaluating the role of PANI morphology on electrochemical properties in a noticeable manner is of great significance.

Herein, a subtle method of tuning PANI dimension is reported. Aniline polymerization proceeds in the identical experimental conditions in addition to using different kinds of additive surfactants. The same conditions can be capable of eliminating the impacts of objective factors as much as possible. Distinct PANI morphologies of fiberboards, dendrites, and rods are botained by adding sodium dodecyl sulfonate (SDS), sodium lauryl sulfonate (SLS), and sodium dodecyl benzene sulfonate (SDBS), respectively. It is of great importance that upon simply introducing surfactants with different end group substitutions, dimension variation is realized for the resulting PANI structures. The formation mechanism and the PANI morphology dependent electrochemical performances are studied in details. The significance of end group substitutions to the morphology difference is also illuminated.

2. Experimental section

2.1. Materials

Aniline monomer (Hongyan Chemical Reagent Co., Ltd.) was purified through distillation under reduced pressure and stored in a refrigerator before use. Hydrochloric acid (HCl; Beijing Chemical Works), sodium dodecyl sulfonate (SDS; Kemiou Chemical Reagent Co., Ltd.), sodium lauryl sulfonate (SLS; China National Pharmaceutical Industry Co., Ltd.), sodium dodecyl benzene sulfonate (SDBS; Fuchen Chemical Reagent Co., Ltd.), ammonium persulfate (APS; Hongyan Chemical Reagent Co., Ltd.), and absolute ethanol (Fuyu Chemical Reagent Co., Ltd.) were of analytical grade and utilized as received. Deionized water was applied throughout all the preparation processes. The ball-and-stick model of SDS, SLS, and SDBS molecules and their corresponding abbreviated sticks model is illustrated in Scheme 1.

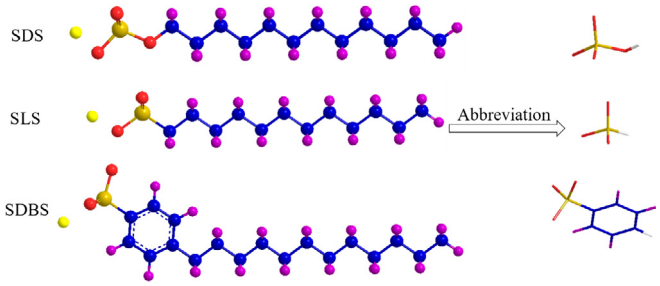

Scheme 1. Ball-and-stick model of SDS, SLS, and SDBS molecules and their corresponding abbreviated sticks model.

2.2. PANI synthesis in the presence of surfactants

Three PANI structures including fiberboards, dendrites, and rods were developed with adding different surfactants. In a typical run, 0.30 mL purified aniline and 0.10 g SDS, SLS, or SDBS were fully dispersed in a 90 mL, 0.010 M HCl solution to form a homogeneous mixture via 30 min ultrasound. Then 10 mL HCl solution (0.010 M) containing 164.2 mg APS was poured into the above mixture to initiate polymerization. The reaction was remained still at room temperature for 10 h. The sediment was thoroughly suction filtered with ethanol and deionized water several times and dried in vacuum oven at 70 °C for 12 h. The purified PANI samples were obtained.

2.3. Characterization

Field emission scanning electron microscopy (FE-SEM) images were generated with a ZEISS MERLIN microscope. Transmission electron microscopy (TEM) images were recorded on a JEOL JEM-3010 microscope with Oxford 794-CCD camera at an accelerating voltage of 200 kV. The samples suspended in ethanol were dropped onto copper grids covered with a carbon support film before observation. The samples dispersed in ethanol were deposited onto silicon wafers and sputtered with platinum by a JFC-1600 auto fine coater at a 20 mA current for 300 s prior to observation. Fourier transform infrared spectra (FTIR) were obtained from a Bruker TENSOR 27 spectrometer. X-ray diffraction patterns (XRD) were determined on a Shimadzu XRD-7000S diffractometer from 5.0 to 40°. X-ray photoelectron spectra (XPS) were obtained via using a Kratos Axis Ultra DDL spectrometer.

Cyclic voltammetry (CV), galvanostatic charge-discharge (GCD), and electrochemical impedance spectroscopy (EIS) curves were carried out in 1.0 M H_2SO_4 solution by applying a Princeton Applied Research VersaSTAT 4 three-electrode electrochemical workstation. A glassy carbon electrode having a diameter of 3 mm with samples on its surface acted as the working electrode. Typically, 5.0 mg sample was ultrasonically dispersed in 1.0 mL naphthol (30 wt%) solution. 5.0 mL of the above solution was added onto the glassy carbon electrode using a pipette and dried at room temperature. Platinum wire acted as the counter electrode. Saturated calomel electrode (SCE) worked as the reference electrode. The CV curves were done within a voltage range of −0.20-0.80 V at a scan rate of 60 mV S^{-1}. The GCD curves were tested at 2.0 A g^{-1} in the switching potential range of 0.0–0.80 V. The EIS curves were measured from 0.010 to 100 Hz with an applied amplitude of 5.0 mV.

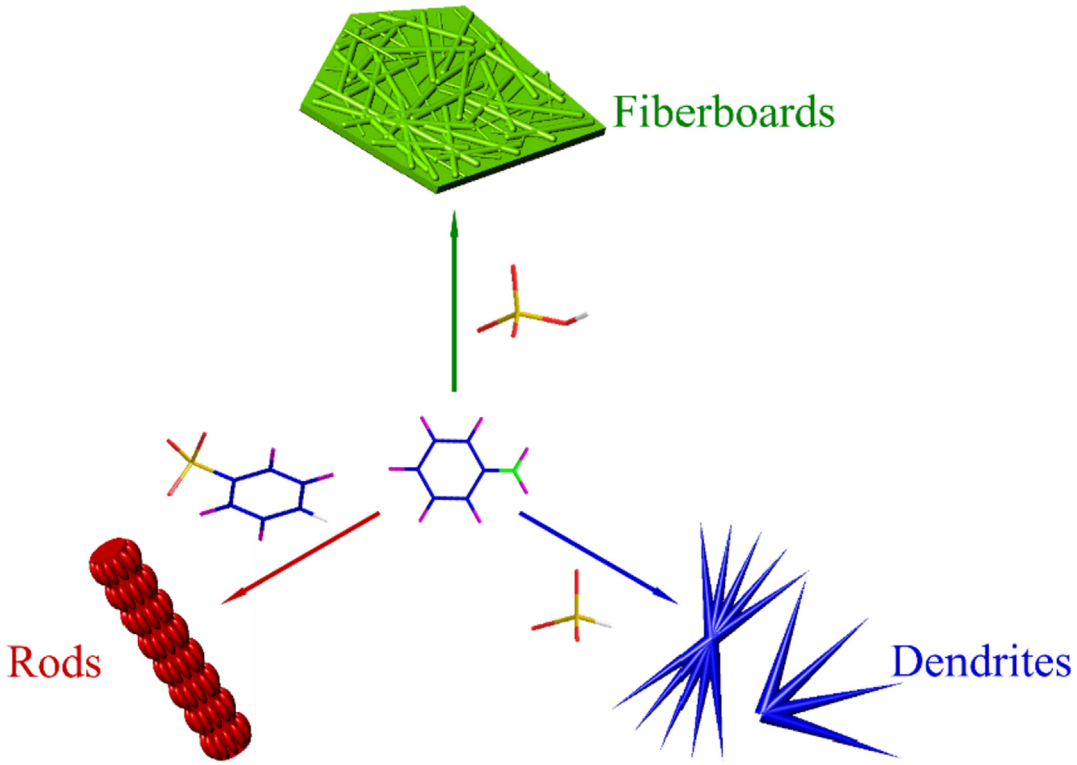

Fig. 1. Schematic representation of dimension tuning of PANI by using surfactants with different end group substitutions.

3. Results and discussion

3.1. Morphology

The schematic illustration of dimension tuning of PANI is shown in Fig. 1. Purified aniline and different surfactants (SDS, SLS, and SDBS) are fully mixed in a low concentration HCl solution (0.010 M). After adding oxidant APS, the polymerization is conducted. With the aid of surfactant molecules, PANI molecules start to assemble. As time passes, amazingly, PANI fiberboards, dendrites, and rods are separately constructed. It is noteworthy that all polymerizations are remained undisturbed, since unstill behaviors (such as shaking or stirring) can dilute local concentration or even destroy transient ordered regions of freshly formed PANI molecules, thereby disturbing their growth and self-assembly process, and then deteriorating dimension tuning [35]. Moreover, there is no demand for cooling the synthetic process, therefore, electric energy is saved along with a remarkable reduction in the equipment cost.

Electron microscope images of distinct PANI structures are shown in Fig. 2. In the case of using SDS, various shaped PANI fiberboards with a size up to tens of microns are prepared, as shown in SEM image of Fig. 2 (a). SEM image of Fig. 2 (b) displays the detailed composition of a fiberboard, in which the crossing nanofibers with a diameter of 50–130 nm are compactly stacked and fused with each other, meanwhile, accompanied by tons of holes having 70–170 nm in diameter among nanofibers. From TEM image of Fig. 2 (c), it can be further demonstrated that the fiberboards not only consist of nanofibers, but also have pores in their body. In SEM image of Fig. 2 (d), for the situation of adding SLS, PANI dendrites dominate the final morphology. Branches composing of dendrites have 0.30–1.5 μm in diameter and 4.0–10.0 μm in length, resulting in a large aspect ratio. The SEM image of Fig. 2 (e) with a high magnification reveals the branches of dendrites from the tip to the fixed end without noticeable change of surface morphology. In TEM image of Fig. 2 (f), one can find branches having sharp tip and solid structure. With respect to the employment of SDBS, PANI rods with 1.5–2.5 μm in diameter and 8.0–20.0 μm in length, and concurrently a handful of nanofibers are viewed in SEM image of Fig. 2 (g). The SEM image of Fig. 2 (h) exhibits magnified rod possessing rough surface, which convincingly confirms the occurrence of secondary growth (the newly formed PANI molecules growing on the surface of already rods). From TEM image of Fig. 2 (i), solid structure and rough periphery are easily discerned.

3.2. Characterization

Fig. 3 (a) exhibits FTIR spectra of PANI fiberboards, dendrites, and rods, respectively. In these spectra, the peaks at 2925 and 2853 cm^{-1} correspond to the N-H stretching vibrations of secondary amines. The peaks at 1566 and 1507 cm^{-1} are separately designated to the C=C stretching deformation of quinonoid and benzenoid rings. There are two sharp peaks owing to C-N and C=N stretching vibrations with aromatic conjugation at 1231 and 1129 cm^{-1}. The peaks at 991 and 744 cm^{-1} result from the C-H in plane and out of plane deformation [36,37]. Judging from FTIR spectra, it is evident that the synthesized samples are made up of PANI molecules.

The crystallinity of three samples is presented through XRD patterns, as shown in Fig. 3 (b). One sharp peak at 6.4° is related to periodic distance between N atom and hydrochloric acid on adjacent main chains. The peaks at 18.3 and 25.7° are separately ascribed to the periodicity in the direction parallel and perpendicular to the PANI molecular chains [38]. However, for fiberboards and dendrites, the peak at 25.7° is not obvious. These displayed data indicate that the synthesized samples have partly crystalline structure. Except for three typical characteristic peaks, several peaks are noted in the fiberboards including those at 8.5, 12.8, 14.9, 20.2, 21.5, 23.4, 24.1°, dendrites including those at 9.1, 11.7, 13.6, 15.9, 16.6, 20.6, 22.9°, and rods including those at 19.5, 23.4, 26.5°. The formation of these extra peaks is attributed to residual surfactants of SDS, SLS, and SDBS.

More detailed information on the composition of the PANI samples can be acquired by XPS spectra in Fig. 4. From Fig. 4 (a), the peaks of oxygen, nitrogen, carbon, and sulfur are detected, meaning the presence of residual surfactants. Besides, imine nitrogen atoms are

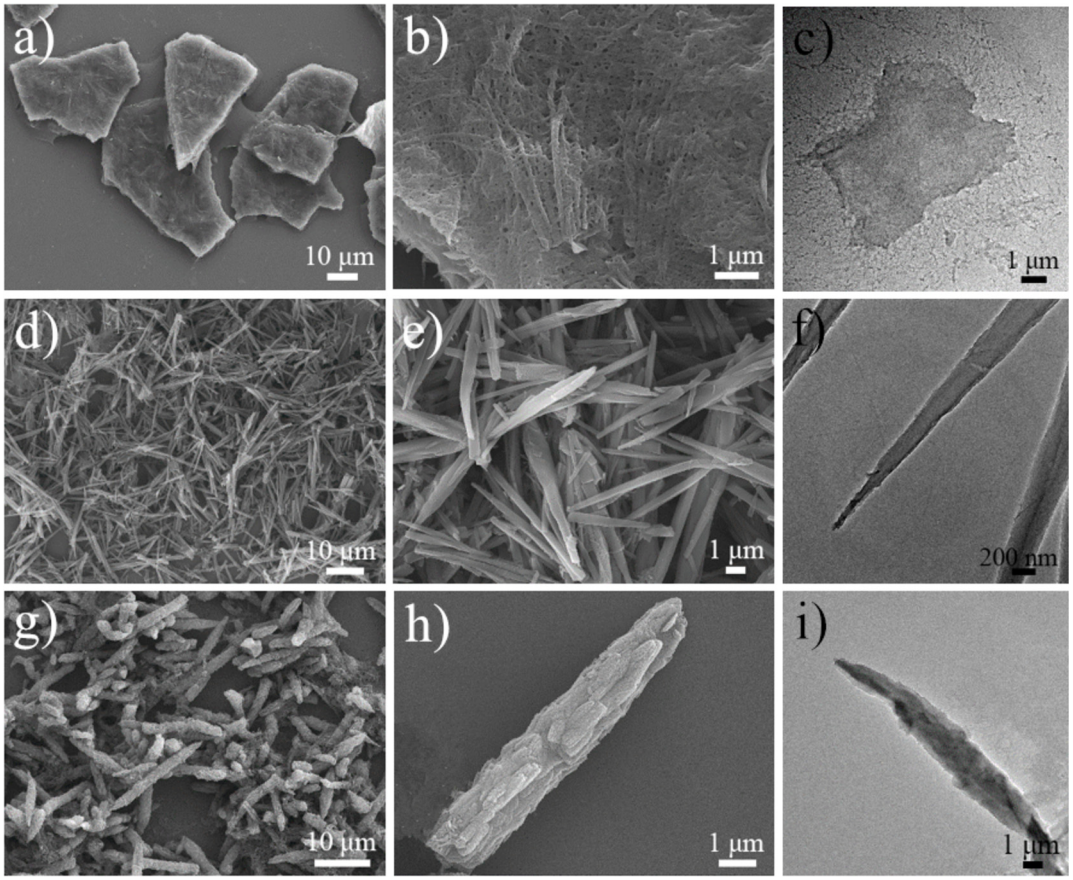

Fig. 2. (a) (b) SEM and **(c)** TEM images of PANI fiberboards, **(d) (e)** SEM and **(f)** TEM images of PANI dendrites, and **(g) (h)** SEM and **(i)** TEM images of PANI rods separately prepared in the presence of SDS, SLS, and SDBS at different magnifications.

protonated to yield a series of oxidation states. As a result, oxidation states of the related PANI samples are quantitatively differentiated by checking the binding energy spectra of nitrogen atoms. Fig. 4 (b, c &d) shows the representative N 1s core-level spectra of PANI fiberboards, dendrites, and rods, respectively. Each spectrum is deconvoluted into three major parts with the binding energy at 399.7, 398.9, 397.2 eV (fiberboards), 399.6, 398.9, 397.0 eV (dendrites), 398.2, 396.7, 395.2 eV (rods), successively stemming from positively charged nitrogen (-N^+-), benzenoid amine (-NH-), and quinonoid imine (=N-). The atomic ratio is summarized in Table 1. It is clear that the ratios of –the N^+-, -NH-, and = N- for the corresponding samples are 28.66, 53.14, 18.20% (fiberboards); 14.41, 49.39, 36.20% (dendrties); and 33.97, 55.02, 11.01% (rods). From these data, the proportions of emeraldine base are calculated to be 46.86, 50.61, and 45.92%, unambiguously suggesting that these three samples have a potential to reach a high doping level and have good conductivity.

3.3. Mechanism

Fig. 5 shows the micelle soft template mechanism responsible for the formation of PANI structures. In the reaction system, under ultrasound, it is reasonable to understand that the micelles consisting of SDS,

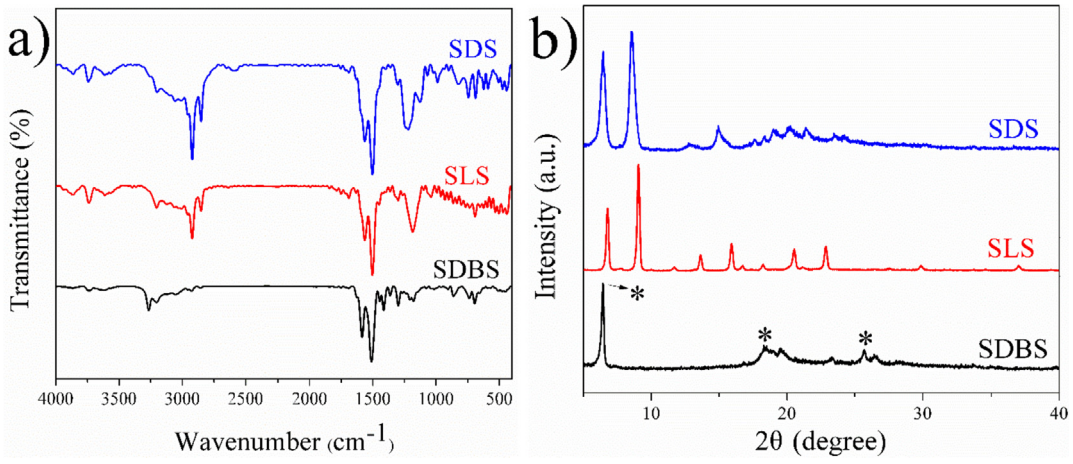

Fig. 3. (a) FTIR spectra and **(b)** XRD patterns of PANI fiberboards, dendrites, and rods prepared in the presence of SDS, SLS, and SDBS, respectively.

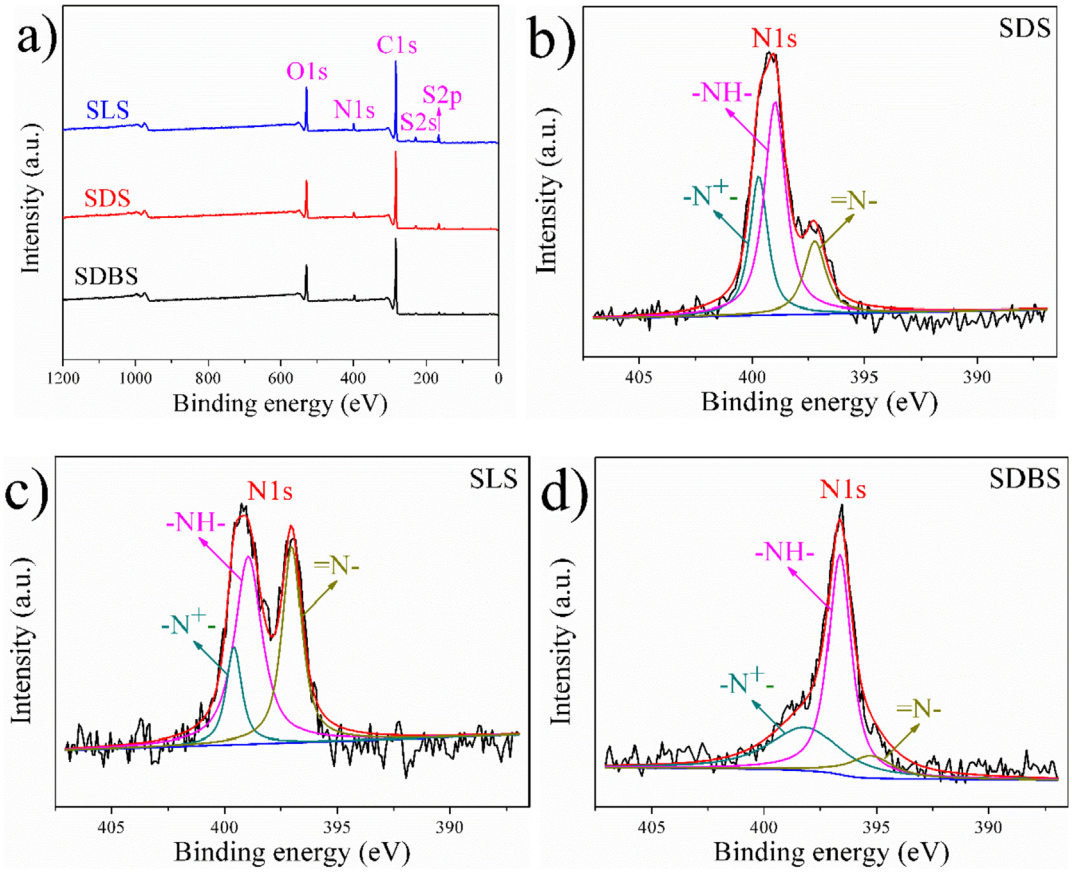

Fig. 4. (a) XPS spectra of PANI fiberboards, dendrites, and rods prepared in the presence of SDS, SLS, and SDBS, respectively. N 1s core-level spectra of PANI **(b)** fiberboards, **(c)** dendrites, and **(d)** rods.

Table 1
XPS atomic ratio of PANI fiberboards, dendrites, and rods prepared in the presence of SDS, SLS, and SDBS, respectively.

PANI structures	$-N^+-$ (%)	-NH- (%)	= N- (%)
Fiberboards	28.66	53.14	18.20
Dendrites	14.41	49.39	36.20
Rods	33.97	55.02	11.01

SLS, or SDBS molecules are easily formed, because of their amphipathicity. Furthermore, these tubular micelles can be readily maintained for the purpose of lowering the surface energy between micelle molecules and solvent molecules [36]. Afterwards, aniline molecules enter into the inside of the micelles due to similar compatibility. These aniline-filled micelles serve as soft templates for polymerization. At first, micelle-solvent interface witnesses aniline polymerization after adding oxidant APS. Subsequently, polymerization takes place in the interior of the micelles. As time goes on, tubular micelles are transformed into 1D PANI nanostructures. During the process, of particular attention is that the surfactant molecules used herein possess much longer alkyl chain than that of perfluorocarbon sulfonic acid [39], azobenzenesulfonic acid [40], and rhodamine B [41] utilized in producing hollow structures of conducting polymers. Therefore, SDS, SLS, and SDBS micelles have a better solubilization effect and more aniline

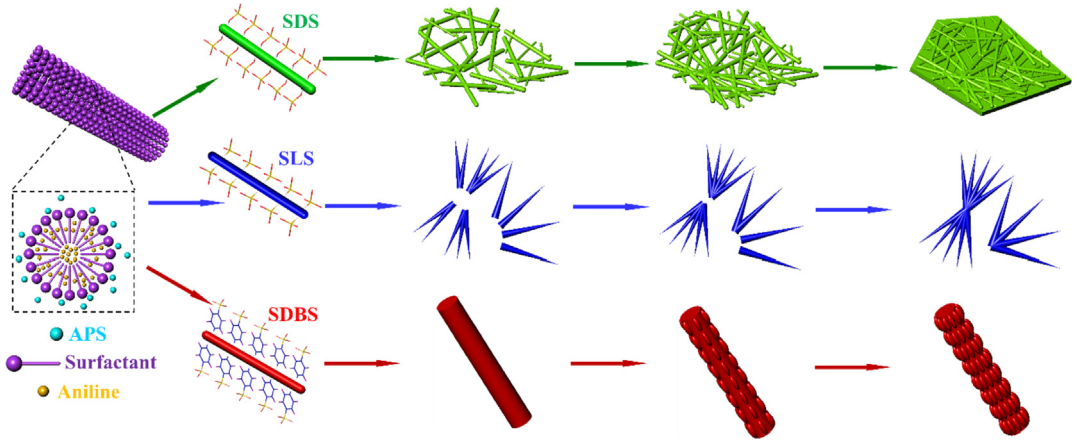

Fig. 5. Schematic representation of fabrication mechanism of PANI fiberboards, dendrites, and rods prepared in the presence of SDS, SLS, and SDBS, respectively.

molecules are adsorbed to their interior, giving birth to the 1D PANI nanostructures with solid structures. On the other hand, surfactant molecules can stabilize these freshly synthetic 1D nanostructures.

With regards to employing SDS, since hydrophilic groups of SDS molecule get one additional oxygen, hydrogen bonding can be spontaneously built among 1D PANI nanostructures with abundant SDS molecules on their surface. These 1D nanostructures are subsequently assembled under hydrogen bonding. With the reaction proceeding, this nanostructure will be fused with each other, forming the fiberboards. In the fusion process, disordered accumulation of 1D nanostructures causes the formation of pores on the fiberboards. In the case of applying SDBS, hydrophilic group of SDBS molecule has bulky phenyl groups. Steric hindrance of these phenyl groups keeps 1D nanostructures independent of each other. During the growth of single 1D nanostructures, secondary growth takes place preferentially and successively in the proximity of already formed 1D nanostructures on account of low nucleation energy [42]. Accordingly, 1D nanostructures are swept across by new nucleation centers of PANI, and followed by the formation of a rough surface. Towards using SLS, due to the lack of one additional oxygen, reduction in the number of hydrogen bonding effectively avoids attracting the 1D nanostructures, remarkably increasing their mobility. Nevertheless, the disappearance of steric hindrance attributed to the nonexistent phenyl group increases the collision and combination probability of 1D nanostructures. On the basis of the synergistic effect, PANI dendrites are established. As the reaction proceeds, each 1D nanostructure grows up into branches and along with the formation of a sharp tip.

3.4. Electrochemical performances

The electrochemical performances of these three PANI samples are characterized in Fig. 6. The counter electrode and the reference electrode are platinum electrode and saturated calomel electrode (SCE), respectively. Fig. 6 (a) shows the CV curves of these samples measured in 1.0 M H_2SO_4 solution between −0.20 and 0.80 V. All curves indicate a typical pseudocapacitive behavior, and demonstrate three pairs of redox peaks, marked by C1/A1, C2/A2, and C3/A3. The first and third pairs are relative to the transformation of PANI molecules from lucoemeraldine to emeraldine and from emeraldine to pernigraniline [43]. The C2/A2 of small humps in the range of 0.50–0.60 V is ascribed to the overoxidation of PANI, which is commonly viewed with reactions occurring in the aqueous electrolytes [44]. What's more, the CV curve of rods displays a larger area than that of other samples, which suggests that the rods possess the best capacitance performance. The charge-discharge behavior is investigated by scrutinizing GCD curves measured at a current density of 2.0 A g^{-1} from 0.0 V to 0.80 V, to botain the specific capacitance of the samples [45]. In Fig. 6 (b), all GCD curves have shapes resembling near-equilateral triangles. The near linear charge and discharge slopes mean superior reversibility during the charge-discharge processes. In the meantime, all the curves have the IR drop at the beginning of the discharge process, which is caused by the internal resistance.

The specific capacitance was calculated according to formula (1) [46]:

$$C_s = \frac{I \times \Delta t}{\Delta V \times m} \quad (1)$$

where C_s (F g^{-1}) denotes the specific capacitance, I (A) denotes the charge-discharge current, Δt (s) denotes the discharge time, ΔV (V) denotes the voltage window for discharge process, and m (g) denotes the mass of active materials. The discharging time increases in the order of fiberboards (SDS) < dendrites (SLS) < rods (SDBS) over the

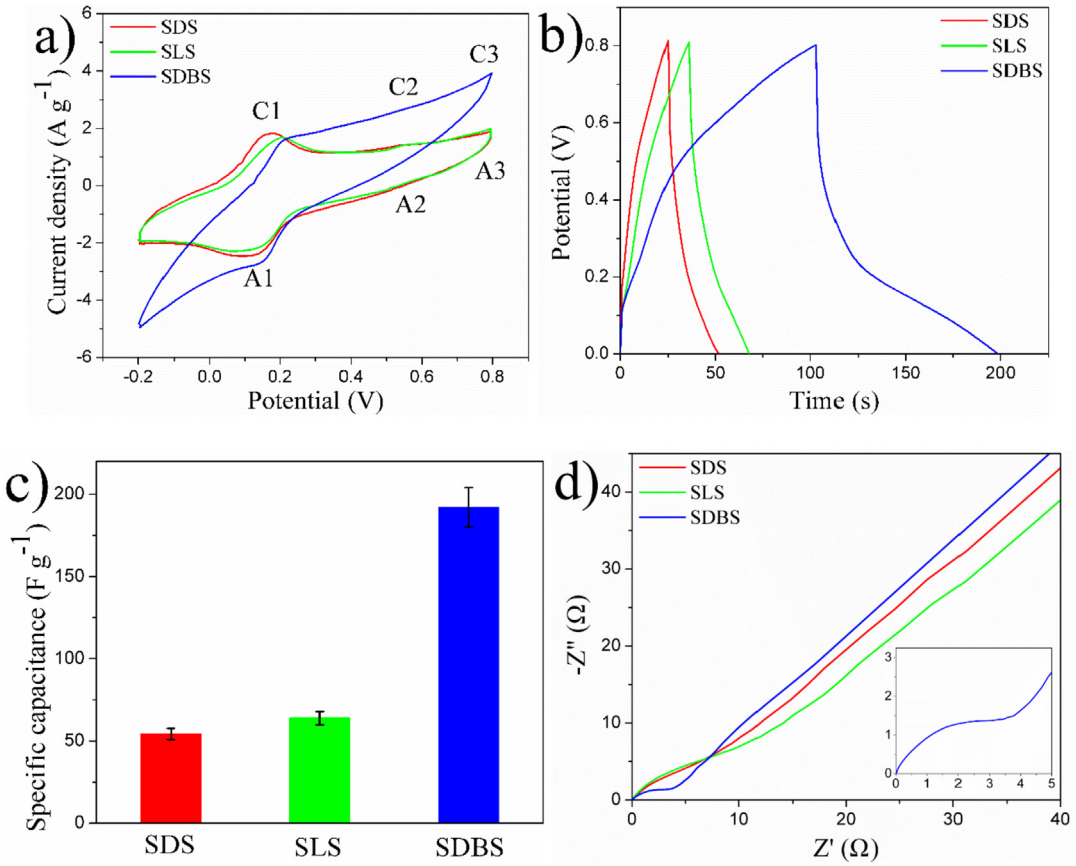

Fig. 6. (a) CV curves, **(b)** GCD curves tested at the current density of 2.0 A g^{-1}, **(c)** specific capacitances, and (d) Nyquist plot and corresponding enlarging view in high-frequency region of PANI fiberboards, dendrites, and rods prepared in the presence of SDS, SLS, and SDBS, respectively.

identical potential range, implying that the rods have the highest specific capacitance. After calculation, the specific capacitance is 55, 64, and 192 F g^{-1}, respectively.

The difference in specific capacitances is mainly a result of the PANI morphology difference. It is well-known that the morphology of materials has a great influence on the final electrochemical properties [47]. Here, the rods have 1D structure and coarse surface, which are beneficial to construct conductive path and possess high specific surface area, forcefully favoring not only the transportation of the charges but also the contact of the electrolyte. This structure reduces the diffusion path of ions, strengthens the electroactive regions, and increases the kinetics of ions. However, for fiberboards, they have a 3D block structure. It is hard for these blocks to build a conductive path in the stacking process. As for dendrites, although these structures with two-dimensional branches can readily form a conductive path, the smooth surface has the disadvantage in terms of improving the specific surface area. This is adverse for the effective contact of ions. Hence, fiebrboards and dendrites display inferior specific capacitance.

To further reveal the electronic conductivity of three PANI samples during the redox process, the Nyquist plots are shown in Fig. 6 (d). It is noted that each curve composes of a straight line and a semicircle at the low frequency region and the high frequency region, respectively. The semicircle of PANI rods can be better viewed from the inset image. The charge transfer resistance (R_{ct}) of three PANI samples is successively 7.40, 7.29, and 3.69 Ω, based on the arc radius of the high frequency region on the real axis. These values demonstrate that the conductivity ability is in the order of fiberboards (SDS) < dendrites (SLS) < rods (SDBS), in accordance with the result of the specific capacitance. Such difference in conductivity on one hand originates from the variation of inherent morphology, on the other hand is affected by the residual surfactant molecules. From the aforementioned XRD patterns, there is the smallest amount of surfactant molecules left in the body of the rods. The inclined lines represent the Warburg impedance attributed to proton diffusion in host materials and electrolyte diffusion in electrode [48]. By means of discussing the electrochemical data of these three PANI samples, it is found that the PANI electrochemical performances have a morphological dependence. Therefore, through simply controlling the morphology of the materials, the tuning and even controlling the resulting properties can be readily realized.

4. Conclusions

By using micelle soft templates consisting of various surfactants (SDS, SLS, or SDBS) with different end group substitutions, the dimension of the as-prepared PANI can be totally tuned, i.e., PANI fiberboards, dendrites, and rods are separately fabricated. The growth process of these PANI structures undergoes a bottom-up self-assembly behavior where 1D nanostructures are gathered into higher order architectures. Electrochemical performances of these structures indicate the morphological dependent behaviors. The specific capacitance of rods (192 F g^{-1}) is the highest in comparison with that of fiberboards and dendrites. The reason is that rods have a high specific surface area and rougher surface, which are beneficial to sufficient contact between ions and active sites. The approach presented herein comes up with a striking way for tuning PANI dimension, and then affects the electrochemical performances. Moreover, with a much lighter weight as compared with metals and ceramics [49–58], it should stimulate further exploration about dimension tuning of other conducting polymers for other applications such as electromagnetic interference (EMI) shielding [59–65], energy storage [66,67], sensors [68], adsorbents for removing heavy metal and other pollutants [69–78] and fillers to make structural and functional nanocomposites [79–93] as well.

Acknowledgment

We gratefully appreciate the support of the National Natural Science Foundation of China (No. 51503116), the Tai'shan Scholar Project of Shandong Province of China (No. TSHW20130956), the National Natural Science Foundation of Shandong (No. ZR2017MA013), and Scientific Research Foundation of Shandong University of Science and Technology for Recruited Talents (No. 2017RCJJ016).

References

[1] H. Wei, D. Cui, J. Ma, et al., J. Mater. Chem. A 5 (2017) 1873–1894.
[2] H. Wang, Z. Xu, H. Yi, H. Wei, Z. Guo, X. Wang, Nano Energy 7 (2014) 86–96.
[3] X. Chen, H. Wang, H. Yi, X. Wang, X. Yan, Z. Guo, J. Phys. Chem. C 118 (2014) 8262–8270.
[4] H. Yi, H. Wang, Y. Jing, et al., J. Mater. Chem. A 3 (2015) 19545–19555.
[5] F. Ran, X. Yang, L. Shao, Adv. Compos. Hybrid Mater. 1 (2018) 32–55.
[6] A. Afzal, F.A. Abuilaiwi, A. Habib, et al., J. Power Sources 352 (2017) 174–186.
[7] H. Zhao, L. Liu, R. Vellacheri, Y. Lei, Adv. Sci. 4 (2017).
[8] R.A. Davoglio, G. Cabello, J.F. Marco, S.R. Biaggio, Electrochim. Acta 261 (2018) 428–435.
[9] X. Yang, C. Liang, T. Ma, Y. Guo, J. Kong, J. Gu, M. Chen, J. Zhu, Adv. Compos. Hybrid Mater. 1 (2018) 207–230.
[10] N.A. Kumar, J.-B. Baek, Chem. Commun. 50 (2014) 6298–6308.
[11] L. Wang, J. Yu, X. Dong, X. Li, Y. Xie, S. Chen, P. Li, H. Hou, Y. Song, ACS Sustain. Chem. Eng. 4 (2016) 1531–1537.
[12] L. O'Neill, C. Johnston, P.S. Grant, J. Power Sources 274 (2015) 907–915.
[13] X. Li, L. Zhang, G. He, Carbon 99 (2016) 514–522.
[14] X. Shi, L. Zhang, J. Cai, G. Cheng, H. Zhang, J. Li, X. Wang, Macromolecules 44 (2011) 4565–4568.
[15] Y. Ma, M. Qiao, Y. Chen, C. Hou, B. Zhang, Q. Zhang, RSC Adv. 5 (2015) 9986–9992.
[16] L. Lyu, J. Liu, H. Liu, C. Liu, Y. Lu, K. Sun, R. Fan, N. Wang, N. Lu, Z. Guo, E.K. Wujcik, Eng. Sci. 2 (2018) 26–42.
[17] Y. Zhao, H. Wei, M. Arowo, X. Yan, W. Wu, J. Chen, Y. Wang, Z. Guo, Phys. Chem. Chem. Phys. 17 (2015) 1498–1502.
[18] Q. Hu, C. Guo, D. Sun, et al., ACS Sustain. Chem. Eng. 5 (2017) 11788–11796.
[19] Q. Hu, D. Sun, Y. Ma, B. Qiu, Z. Guo, Polymer 120 (2017) 236–243.
[20] C.O. Baker, X. Huang, W. Nelson, R.B. Kaner, Chem. Soc. Rev. 46 (2017) 1510–1525.
[21] Z. Niu, J. Liu, L.A. Lee, M.A. Bruckman, D. Zhao, G. Koley, Q. Wang, Nano Lett. 7 (2007) 3729–3733.
[22] J.X. Huang, R.B. Kaner, Chem. Commun. (2006) 367–376.
[23] Z.D. Zujovic, Y. Wang, G.A. Bowmaker, R.B. Kaner, Macromolecules 44 (2011) 2735–2742.
[24] H. Guo, J. Chen, Y. Xu, ACS Macro Lett. 3 (2014) 295–297.
[25] Y. Ma, H. Zhang, C. Hou, et al., J. Mater. Sci. 52 (2017) 2995–3002.
[26] Y. Zhu, J. Li, M. Wan, L. Jiang, Y. Wei, Macromol. Rapid Commun. 28 (2007) 1339–1344.
[27] Y. Yang, Y. Zhang, Z. Wei, Adv. Mater. 25 (2013) 6039–6049.
[28] G. Li, Y. Li, Y. Li, H. Peng, K. Chen, Macromolecules 44 (2011) 9319–9323.
[29] Y. Ma, M. Qiao, C. Hou, et al., RSC Adv. 5 (2015) 103064–103072.
[30] H.D. Tran, D. Li, R.B. Kaner, Adv. Mater. 21 (2009) 1487–1499.
[31] W. Wu, D. Pan, Y. Li, G. Zhao, L. Jing, S. Chen, Electrochim. Acta 152 (2015) 126–134.
[32] L. Ren, G. Zhang, Z. Yan, L. Kang, H. Xu, F. Shi, Z. Lei, Z.-H. Liu, ACS Appl. Mater. Interfaces 7 (2015) 28294–28302.
[33] N. Jabeen, Q. Xia, M. Yang, H. Xia, ACS Appl. Mater. Interfaces 8 (2016) 6093–6100.
[34] Y. Liu, Y. Ma, S. Guang, H. Xu, X. Su, J. Mater. Chem. A 2 (2014) 813–823.
[35] Y. Ma, Y. Chen, A. Mei, et al., Chem. Asian J. 11 (2016) 93–101.
[36] Y. Ma, C. Zhang, C. Hou, H. Zhang, H. Zhang, Q. Zhang, Z. Guo, Polymer 117 (2017) 30–36.
[37] Y. Ma, Y. Chen, C. Hou, H. Zhang, M. Qiao, H. Zhang, Q. Zhang, Sci. Rep. 6 (2016).
[38] Y. Ma, C. Hou, H. Zhang, H. Zhang, Q. Zhang, Synthetic Met 222 (2016) 388–392.
[39] Y. Zhu, D. Hu, M. Wan, L. Jiang, Y. Wei, Adv. Mater. 19 (2007) 2092–2096.
[40] P. Anilkumar, M. Jayakannan, Macromolecules 41 (2008) 7706–7715.
[41] Y. Xue, X. Lu, Y. Xu, X. Bian, L. Kong, C. Wang, Polym. Chem. 1 (2010) 1602–1605.
[42] C.-L. Zhu, S.-W. Chou, S.-F. He, W.-N. Liao, C.-C. Chen, Nanotechnology 18 (2007) 275604.
[43] D. Vonlanthen, P. Lazarev, K.A. See, F. Wudl, A.J. Heeger, Adv. Mater. 26 (2014) 5095–5100.
[44] Y. Tian, S. Cong, W. Su, H. Chen, Q. Li, F. Geng, Z. Zhao, Nano Lett. 14 (2014) 2150–2156.
[45] Y. Ma, C. Hou, H. Zhang, M. Qiao, Y. Chen, H. Zhang, Q. Zhang, Z. Guo, J. Mater. Chem. A 5 (2017) 14041–14052.
[46] J. Zhu, M. Chen, H. Qu, Z. Luo, S. Wu, H.A. Colorado, S. Wei, Z. Guo, Energy Environ. Sci. 6 (2013) 194–204.
[47] L. Han, P. Tang, L. Zhang, Nano Energy 7 (2014) 42–51.
[48] H. Wei, H. Gu, J. Guo, D. Cui, X. Yan, J. Liu, D. Cao, X. Wang, S. Wei, Z. Guo, Adv. Compos. Hybrid Mater. 1 (2018) 127–134.
[49] Z. Zhao, R. Guan, J. Zhang, Z. Zhao, P. Bai, Acta Metall. Sin. (Engl. Lett.) 30 (2017) 66–72.
[50] Z. Sun, et al., CrystEngComm 19 (2017) 3288–3298.
[51] Z. Zhao, P. Bai1, R. Guan, et al., Mater. Sci. Eng., A 734 (2018) 200–209.
[52] L. Zhang, W. Yu, C. Han, et al., J. Electrochem. Soc. 164 (2017) H651–H656.

[53] B. Song, T. Wang, H. Sun, et al., Dalton Trans. 46 (2017) 15769–15777.
[54] X. Lou, C. Lin, Q. Luo, et al., ChemElectroChem 4 (2017) 3171–3180.
[55] C. Lin, H. Hu, C. Cheng, et al., Electrochim. Acta 260 (2018) 65–72.
[56] Q. Hou, J. Ren, H. Chen, et al., ChemElectroChem 5 (2018) 726–731.
[57] Y. Zhao, L. Qi, Y. Jin, et al., J. Alloy. Comp. 647 (2015) 1104–1110.
[58] Y. Zhao, S. Deng, H. Liu, et al., Comput. Mater. Sci. 154 (2018) 365–370.
[59] N. Wu, C. Liu, D. Xu, et al., ACS Sustain. Chem. Eng. 6 (2018) 12471–12480.
[60] Z. Wang, R. Wei, J. Gu, et al., Carbon 139 (2018) 1126–1135.
[61] C. Wang, V. Murugadoss, J. Kong, et al., Carbon 140 (2018) 696–733.
[62] P. Xie, B. He, F. Dang, et al., J. Mater. Chem. C 6 (2018) 8812–8822.
[63] J. Guo, H. Song, H. Liu, et al., J. Mater. Chem. C 5 (2017) 5334–5344.
[64] K. Zhang, G. Li, L. Feng, et al., J. Mater. Chem. C 5 (2017) 9359–9369.
[65] J. Gu, W. Dong, Y. Tang, et al., J. Mater. Chem. C 5 (2017) 6929–6936.
[66] B. Kirubasankar, V. Murugadoss, J. Lin, et al., Nanoscale (2018), https://doi.org/10.1039/C8NR06345A in press.
[67] W. Deng, T. Kang, H. Liu, et al., Sci. Adv. Mater. 10 (2018) 937–949.
[68] H. Gu, H. Zhang, J. Lin, et al., Polymer 143 (2018) 324–330.
[69] Y. Li, T. Jing, G. Xu, et al., Polymer 149 (2018) 13–22.
[70] Y. Ma, L. Lyu, Y. Guo, et al., Polymer 128 (2017) 12–23.
[71] Y. Wang, P. Zhou, S. Luo, et al., Langmuir 34 (2018) 7859–7868.
[72] K. Gong, Q. Hu, L. Yao, et al., ACS Sustain. Chem. Eng. 6 (2018) 7283–7291.
[73] J. Huang, Y. Cao, Q. Shao, et al., Ind. Eng. Chem. Res. 56 (2017) 10689–10701.
[74] S. Sun, L. Zhu, X. Liu, et al., ACS Sustain. Chem. Eng. 6 (2018) 9866–9875.
[75] K. Gong, Q. Hu, Y. Xiao, et al., J. Mater. Chem. A 6 (2018) 11119–11128.
[76] Z. Li, B. Wang, X. Qin, et al., ACS Sustain. Chem. Eng. (2018), https://doi.org/10.1021/acssuschemeng.8b01637 in press.
[77] J. Huang, Y. Li, Y. Cao, et al., J. Mater. Chem. A 6 (2018) 13062–13074.
[78] K. Gong, S. Guo, Y. Zhao, et al., J. Mater. Chem. A (2018), https://doi.org/10.1039/C8TA06571C in press.
[79] Z. Hu, Q. Shao, Y. Huang, et al., Nanotechnology 29 (2018) 185602.
[80] Y. Guo, G. Xu, X. Yang, et al., J. Mater. Chem. C 6 (2018) 3004–3015.
[81] K. Sun, R. Fan, X. Zhang, et al., An overview of metamaterials and their achievements in wireless power transfer, J. Mater. Chem. C 6 (2018) 2925–2943.
[82] J. Gu, Y. Li, C. Liang, et al., J. Mater. Chem. C 6 (2018) 7652–7660.
[83] B. Zhou, Y. Li, K. Dai, et al., J. Mater. Chem. C 6 (2018) 8360–8371.
[84] B. Song, T. Wang, H. Sun, et al., Compos. Sci. Technol. 167 (2018) 515–521.
[85] Z. Wu, H. Cui, L. Chen, et al., Compos. Sci. Technol. 164 (2018) 195–203.
[86] X. Wang, X. Liu, H. Yuan, et al., Mater. Des. 139 (2018) 372–379.
[87] Y. Lu, M.C. Biswas, Z. Guo, et al., Biosens. Bioelectron. (2018), https://doi.org/10.1016/j.bios.2018.08.037 in press.
[88] Z. Hu, D. Zhang, F. Lu, et al., Macromolecules 51 (2018) 5294–5303.
[89] K. Sun, P. Xie, Z. Wang, et al., Polymer 125 (2017) 50–57.
[90] X. Guo, S. Ge, J. Wang, et al., Polymer 143 (2018) 155–163.
[91] C. Wang, V. Murugadoss, J. Kong, et al., Carbon 140 (2018) 696–733.
[92] H. Du, C. Zhao, J. Lin, et al., Chem. Rec. 18 (2018) 1365–1372.
[93] Z. Hu, C. Wang, F. Zhao, et al., Nanoscale 9 (2017) 8825.